JOURNAL OF MATERIALS SCIENCE **34** (1999) 905–915

Effect of SiO_2 binder on the precipitation state of an AlCu4Mg1Ag/Saffil composite

C. CAYRON, P. A. BUFFAT
Interdepartmental Centre of Electron Microscopy, EPFL, 1015 Lausanne, Switzerland, E-mail: cyril.cayron@epfl.ch

O. BEFFORT, S. LONG
Swiss Federal Institute for Materials Testing and Research, EMPA, 3602 Thun, Switzerland

The microstructure of an AlCu4Mg1Ag alloy reinforced with 15 vol % Al_2O_3-Saffil fibers was investigated by analytical transmission electron microscopy and compared to the microstructure of the unreinforced alloy. The investigation results show that the composite matrix is enriched in Si as a consequence of the interfacial reaction between the Mg from the alloy and the SiO_2 from the fiber and fiber binder. The presence of Si in the composite matrix modifies the characteristic precipitation state of the monolithic Al-alloy: in the peak aged T6-temper, the phases $\Omega + S'$ are substituted by a fine and homogeneous precipitation of θ' plates, and a new type of rod-shaped precipitates. On overageing, these rod-shaped precipitates can be classified into two categories: precipitates containing Al, Cu, Mg, and Si (possibly a Q-phase precursor) and Si precipitates that act as nuclei for θ'.

1. Introduction

Light weight metals based metal matrix composites (MMCs), when compared to their monolithic base alloys, typically show improved performance in terms of mechanical properties such as higher Young's modulus, higher service temperature, improved wear resistance, better fatigue resistance, reduced coefficient of thermal expansion, and thus, are very attractive for many engineering applications, for instance in the automotive and aerospace industries [1].

The physical and chemical phenomena occurring at the fiber/matrix interfaces play an important role in the microstructure formation and property development of a wide range of composites [2]. For example, the dislocation density is generally increased in the interface area because of the difference between the coefficient of thermal expansion [3] and the chemical composition can be modified as a consequence of interfacial reactions [4]. All of these aspects may change the precipitation state of the matrix, quantitatively and sometimes qualitatively [5]. Obviously, these microstructure modifications will affect the mechanical properties of the matrix and, therefore, the performance of the MMCs. Therefore, an understanding on the interfacial phenomena and the associated matrix microstructure formation during the MMC's fabrication and subsequent heat treatment is essential for a reliable prediction of their mechanical properties.

In the early stage of the present study, a δ-Al_2O_3 Saffil chopped fiber preform containing 5 wt % silica binder was infiltrated with an AlCu4Mg1Ag alloy by direct squeeze casting, followed by solution heat treatment and peak age hardening. The same monolithic alloy was cast in the same conditions, subjected to the same solution heat treatment and also peak aged. The results of mechanical tests on the composite and unreinforced alloy, as summarized in Table I, indicate an improvement of the Young's modulus and ultimate tensile strength as a consequence of the addition of the Saffil fibers. In contrast, another study on a similar MMC-type, fabricated by liquid metal infiltration, reported a drop of microhardness [6] and only a slight increase of strength [7] with fibers addition. This has been explained by the suppression of the hardening phase Ω, due to the depletion of Mg in the matrix resulting from its reaction with the alumino-silicate binder.

To promote a sound understanding on the improved mechanical behavior of the AlCu4Mg1Ag/Saffil composite of the present study, the microstructure and chemistry of the SiO_2 binder, fiber-matrix interfaces and matrix precipitation features were investigated with analytical transmission electron microscopy (TEM).

2. Experimental procedure

2.1. Material

The preforms used in this study were custom made by Vernaware Ltd, UK, and consist of 15 vol % δ-Al_2O_3 based Saffil chopped fibers (96-97 wt % Al_2O_3, 3-4 wt % SiO_2) with 5 wt % SiO_2 binder. The matrix alloy AlCu4Mg1Ag is based on a well characterized high performance AlCu4MgAgMnZr-wrought alloy described elsewhere [8]. To meet the demands of high strength fibrous MMCs on a matrix alloy (i.e. to avoid embrittling intermetallic phases), the transition elements Mn and Zr of the original AlCu4MgAgMnZr alloy were omitted.

TABLE I Mechanical properties of the AlCu4Mg1Ag/Saffil composite and its unreinforced base alloy (T6-temper)

Material	E (GPa)	$\sigma_{0.02}$ (MPa)	σ (MPa)	σ_{total} (%)	HB	K_{IC} (MPa.m$^{1/2}$)
15% Saffil/AlCu4MgAg	88.70	413.6	517.6	2.6	198	13.8
AlCu4MgAg Alloy	72	413	454	5.4	150	24

TABLE II Effective chemical composition of the reference alloy in wt %

Al	Cu	Mg	Ag	Fe	Si
bal	4.03	1.04	0.53	0.03	0.043

The Mg content was raised to 1 wt % to compensate for its apprehended loss from reaction with the SiO_2-based preform binder because it has been shown that a precise balance of Cu, Mg, and Ag is required for the precipitation of the Ω-phase, to which the good mechanical properties of the alloy have been attributed [8]. The effective chemical composition of the AlCu4Mg1Ag alloy is provided in Table II.

The preform was infiltrated with the AlCu4Mg1Ag alloy melt by direct squeeze casting with the processing parameters as follows: melt superheat 730 °C, preform preheat 650 °C, infiltration speed 10 mm/s, and maximum pressure 130 MPa. The composite casting was subsequently solution heat treated at 480 °C/1.2 h + 500 °C/2 h, followed by cold water quenching. After holding at 25 °C for 100 hours (T4), the casting was peak-aged at 170 °C for 4 h (T6). The resultant microstructure was characterized by a uniform distribution of the Saffil fibers in the matrix alloy free of porosity. The investigations on this composite were carried out in the T6 condition (MMC-T6), but to facilitate the understanding of our TEM analysis of the precipitation state, two overageing treatments were additionally applied at 175 °C for 600 h and 300 °C for 24 h (see section 3.5). To understand the mechanisms of interfacial reactions the MMC in as cast condition (MMC-F) was also studied.

As a reference, the unreinforced alloy was cast in the same conditions and solution heat treated at 480 °C/2 h + 500 °C/2 h, followed by cold water quenching and peak-ageing to T6-condition (T4 + 170 °C/20 h). The age hardening responses of both composite and unreinforced alloy, determined by Brinell HB_{30} hardness measurements, are presented in Fig. 1.

2.2. Experiments

The TEM investigations were performed on a Philips CM20T (LaB_6) operating at 200 kV and equipped with an energy-dispersive spectrometer (EDS) Noran Voyager for standardless chemical analysis. High-resolution electron microscopy (HREM) and EDS analyses at nanometer scale were performed on a Philips CM300UT-FEG operating at 300 kV and on a Hitachi HF2000-FEG.

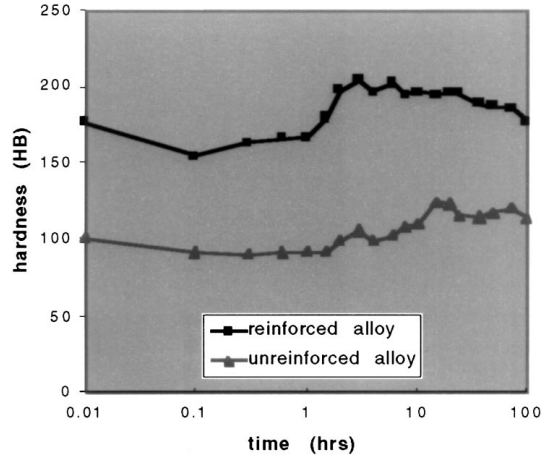

Figure 1 Hardness versus ageing time for the unreinforced alloy and MMC (ageing temperature: 170 °C).

TEM foil specimens were prepared by mechanical dimpling down to 20 μm, followed by argon ion milling on a Gatan Duo-Mill machine, operating at an accelerating voltage of 5 kV and 10° angle, with a liquid nitrogen cooling stage to avoid microstructure changes associated with the annealing effect. Such effects have been experienced on first samples prepared on an ion mill without cooling stage, resulting in an unexpected and substantial coarsening of the precipitation state.

3. Results

3.1. Chemical composition

EDS analysis results on the reference alloy-T6 and in the matrix of the MMC-T6 are provided in Table III. The presence of Si in the MMC matrix is evident, but no reliable results for Mg concentration could be obtained by this method because of the proximity of the small Mg peak to the large Al K_α peak, which results in a very poor deconvolution quality.

Table IV shows the composition of the core of the binder (initially SiO_2) in MMC-F (as cast) (see also section 3.3). As these data suggest, the initial composition of the SiO_2 binder was modified during the MMC infiltration: the binder contains a high level of Mg, and only traces of Si remain. It is obvious that during MMC elaboration, Mg migrates from the matrix into the silica binder, and the Si present in the SiO_2 binder is reduced and ejected into the matrix.

TABLE III Chemical composition (EDS analyses) of the reference alloy-T6 and the MMC-T6 matrix in wt %

	Cu	Mg	Ag	Si
Reference alloy	2.9	2.0 (imprecise)	0.5	0.0
MMC matrix	3	0.1 (imprecise)	0.7	0.6

TABLE IV Chemical composition (EDS analyses) of the binder (initialy SiO_2) in the MMC-F (as cast) composite in at %

	Si	O	Mg	Cu	Al
MMC-F	0.3	38.3	15.4	0.1	45.9

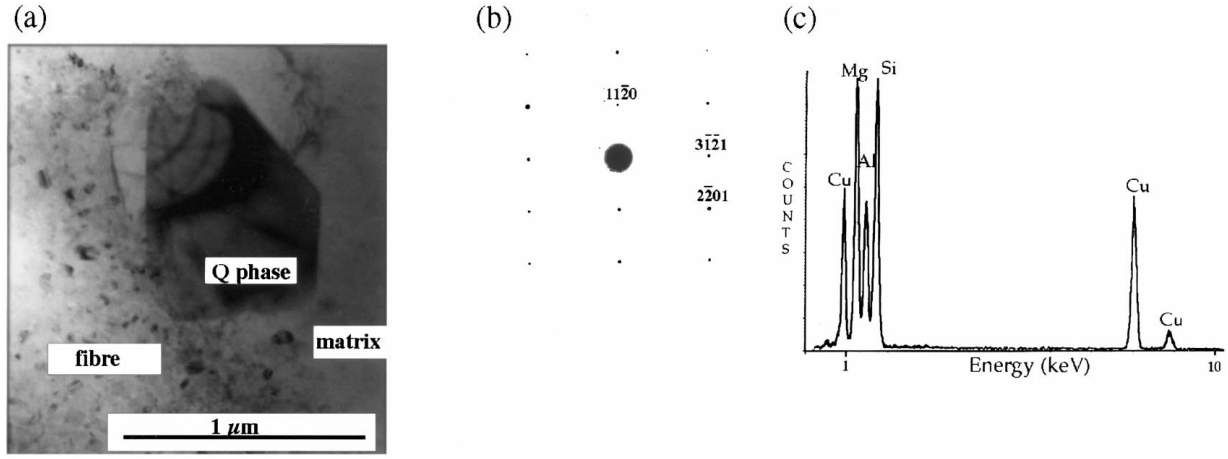

Figure 2 Q precipitate: (a) Bright field image, (b) diffraction pattern in [$1\bar{1}0\bar{4}$] direction and (c) EDS spectrum.

3.2. Coarse intermetallic precipitates

In the MMC-T6, four types of coarse insoluble intermetallic phases have been observed and identified as θ-Al_2Cu, Al_7Cu_2Fe, Q-$Al_5Cu_2Mg_8Si_6$, and $Al_{18}CuSi_2Fe_3$ by EDS analysis and selected-area electron diffraction (SAED).

The θ-Al_2Cu precipitates (tetragonal body centered crystal structure, a = 0.607 nm and c = 0.487 nm) are generally small ($\sim$0.2 μm), globular-shaped, and preferentially appear at the grain boundaries. The Al_7Cu_2Fe precipitates (tetragonal crystal structure, $a = 0.633$ nm and $c = 1.487$ nm) can appear at both grain boundaries (globular shape, 0.5 μm) and fiber-matrix interface (elongated, more than 5 μm long). The formation of this phase is related to matrix alloy Fe-impurities, most probably as the product of a low temperature ternary eutectic reaction [9]:

$$\text{liq} \Rightarrow \text{Al} + \text{Al}_2\text{Cu} + \text{Al}_7\text{Cu}_2\text{Fe}\ (546\,^{\circ}\text{C}) \qquad (1)$$

The θ-Al_2Cu and Al_7Cu_2Fe phases are also found at grain boundaries in the reference alloy-T6. They are a characteristic of the alloy. The two phases containing Si, Q-$Al_5Cu_2Mg_8Si_6$ and $Al_{18}CuSi_2Fe_3$ seem to appear exclusively in the MMC:

3.2.1. Q-$Al_5Cu_2Mg_8Si_6$

As shown in Fig. 2a, the Q-$Al_5Cu_2Mg_8Si_6$ phase usually appears at the fiber-matrix interface with an hexagonal shape ($\sim$1 μm). This phase is known as Q, W, λ, or h with a hexagonal structure ($a = 1.039$ nm and $c = 0.404$ nm) according to the associated reaction type and phase geometry [10–12]. In the present situation, Q-phase is most probably formed during the following reaction [8]:

$$\text{liq} \Rightarrow \text{Al} + \text{Al}_2\text{Cu} + \text{Si} + \text{Al}_5\text{Cu}_2\text{Mg}_8\text{Si}_6\ (510\,^{\circ}\text{C}) \qquad (2)$$

3.2.2. $Al_{18}CuSi_2Fe_3$

As indicated by its EDS spectrum (Fig. 3c), the precipitate shown in Fig. 3a (globular shape, $\sim 0.5\,\mu$m) is formed by the elements Al, Cu, Si, Fe. Quantitative results are given in Table V as atomic ratios from which the stoichiometry of this phase is deduced as $Al_{18}CuSi_2Fe_3$. However, the Al concentration quoted may be overestimated because of the aluminium present in the matrix surrounding this precipitate and exited by the back scattering electrons spiralling in the objective lens magnetic field. The diffraction patterns along several axes (one of which is shown in Fig. 3b) are in good

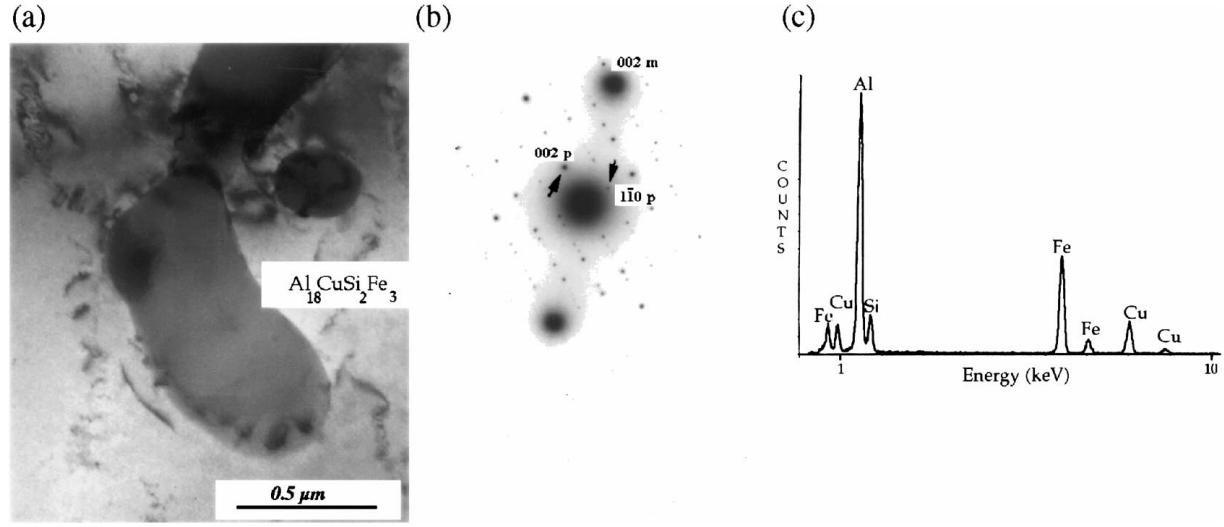

Figure 3 $Al_{18}CuSi_2Fe_3$ precipitate: (a) Bright field image, (b) diffraction pattern in [110] direction (with **m** for the matrix and **p** for the precipitate), and (c) EDS spectrum.

TABLE V Chemical composition of coarse intermetallic precipitates in at % (EDS analyses), atomic ratios deduced, and nominal atomic ratio (for comparison)

	Al_7Cu_2Fe			Q-$Al_5Cu_2Mg_8Si_6$			$Al_{18}CuSi_2Fe_3$	
	at %	ratios	rat. nom.	at %	ratios	rat. nom.	at %	ratios
Al	65.3	10.1	7	15.5	2.00	2.5	68.2	17.7
Mg	—	—	—	36.1	4.67	4	—	—
Si	—	—	—	25.2	3.25	3	7.8	2.04
Cu	13.8	2.12	2	7.7	1	1	3.8	1
Fe	6.5	1	1	—	—	—	11.5	2.98

agreement with a body centered cubic structure with lattice parameter $a = 1.248\ \text{nm} \pm 0.005\ \text{nm}$. To the authors' knowledge, the existence of such a phase has not been reported in literature [13, 14]. The phase with the closest crystal structure is $Al_{12}Fe_3Si$ with a cubic structure and a lattice parameter $a = 1.254$ nm.

Due to their temperature of formation ($> 510\,^{\circ}\text{C}$), these coarse intermetallic precipitates appear before the final solidification in the mushy state and migrate during solidification in interdendritic areas. This is confirmed by TEM analyses on the MMC in the cast condition (F), which reveal the presence of coarse θ-Al_2Cu, Al_7Cu_2Fe, and Q-$Al_5Cu_2Mg_8Si_6$ precipitates, and by the fact that these insoluble particles are found at the grain boundaries or on the fibers (i.e. in the areas of the final solidification).

3.3. Reacted fiber binder

In the MMC-F (as-cast), SAED diffraction patterns have been done on the binder to complete EDS results given in Table IV: they reveal that most of the SiO_2 binder has reacted with Mg to form a spinel $MgAl_2O_4$ with a face-centered cubic structure of $a = 0.8045$ nm, as shown in Fig. 4a, b, and c.

In the MMC-T6, the observations on the surface of the reacted binder or at fiber crossing points reveal the existence of small precipitates (10–100 nm). Two kinds of precipitates could be identified by EDS and SAED: θ-Al_2Cu and spinel $MgAl_2O_4$, as represented in Fig. 5a, b, and c. In the core of the binder, to complete EDS results given in Table IV, diffraction patterns reveal the presence of nanocrystalline MgO as shown in Fig. 5d.

3.4. Matrix precipitation state

3.4.1. The unreinforced AlCu4Mg1Ag-alloy

The precipitation state of the unreinforced AlCu4-Mg1Ag alloy in the T6-condition is characterized by the presence of Ω and S′ as evidenced by identification of the matrix diffraction pattern on $[100]_\alpha$ (Fig. 6; see [8] for diffraction pattern indexation). θ' phase cannot be traced.

3.4.2. The AlCu4Mg1Ag/Saffil MMC

A comparison of the microstructures and the diffraction patterns of the unreinforced alloy (Fig. 6) and the composite matrix (Fig. 7) shows that the precipitation state of the composite matrix substantially differs from the unreinforced alloy. As shown in the following list, the dominant phases observed in the monolithic matrix alloy (Ω and S′) cannot be detected in the composite anymore:

1. The absence of Ω is evidenced by the lack of its characteristic spots in 1/4 (220) position and confirmed by the absence of streaks in {111} directions in the ⟨110⟩ diffraction patterns.

2. The S′ phase is not observed. Indeed the complex $[210]_\alpha$ diffraction pattern, which is often used for S′ identification, can be explained by double diffraction of θ'. Moreover, S phase was not detected in overaged samples.

As shown in Fig. 7, the composite matrix features a fine and dense dispersion of plate- and rod-shaped precipitates. The precipitates were identified as follows:

1. θ' plates appear in the matrix; they are hardly visible in the background of Fig. 7b, but their presence

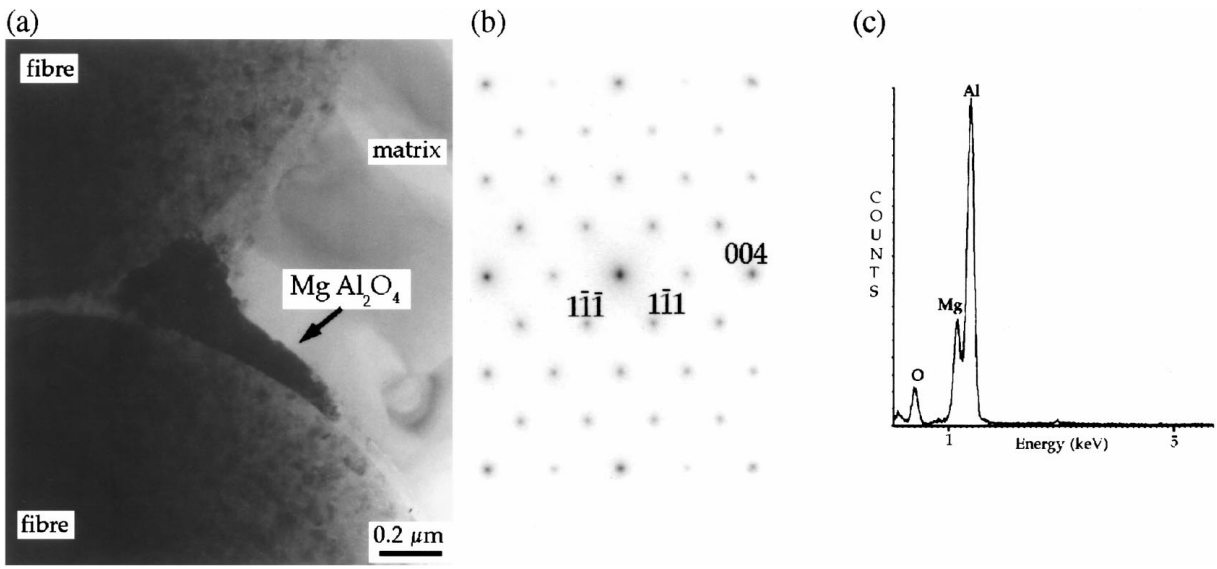

Figure 4 Reacted binder in MMC-F (as cast): $MgAl_2O_4$-spinel precipitates in the reacted binder. (a) Bright field image, (b) diffraction pattern in $[110]_{spinel}$, and (c) EDS spectrum.

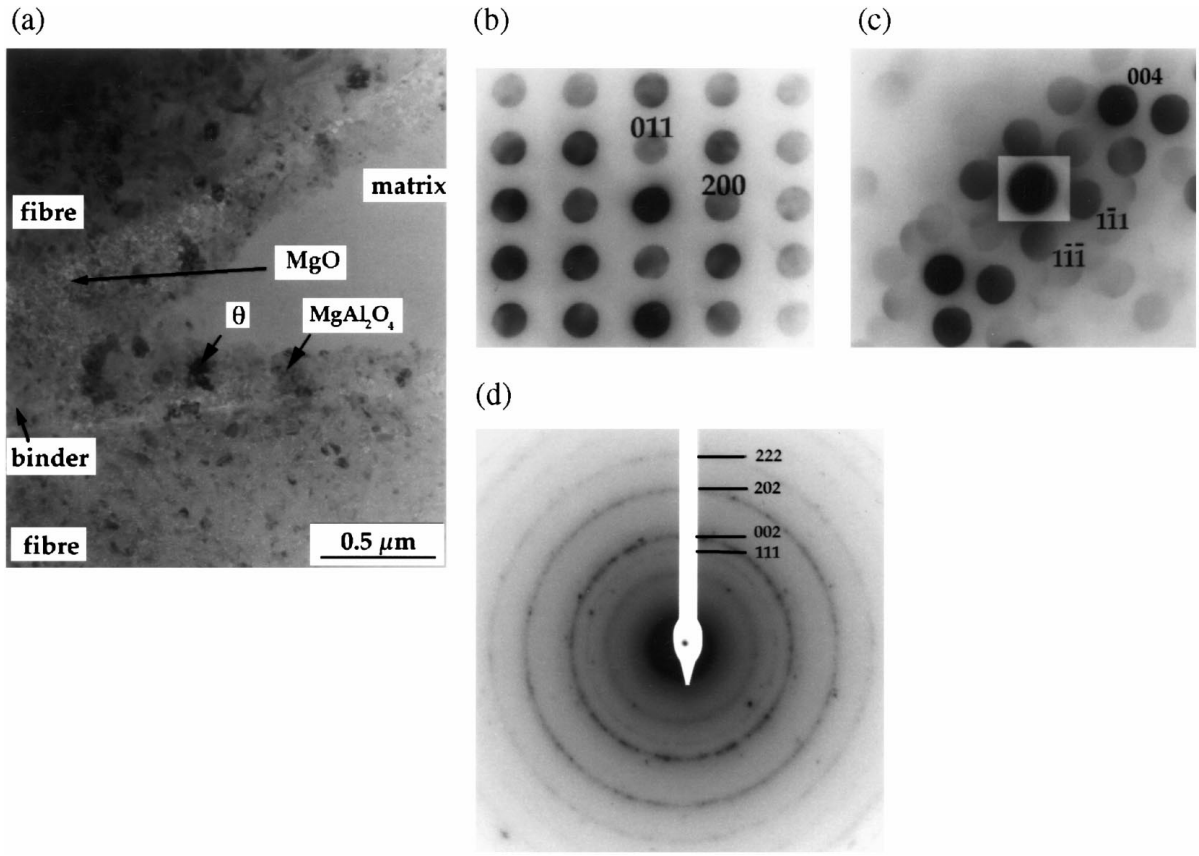

Figure 5 Reacted binder in the MMC-T6: θ-$CuAl_2$, and $MgAl_2O_4$-spinel precipitates around the binder and polycrystalline MgO inside the binder: (a) Bright field image, (b) θ-$CuAl_2$ diffraction pattern in $[01\bar{1}]_\theta$, (c) $MgAl_2O_4$ diffraction pattern $[110]_{\text{spinel}}$ zone axes, and (d) diffraction rings of polycrystalline MgO.

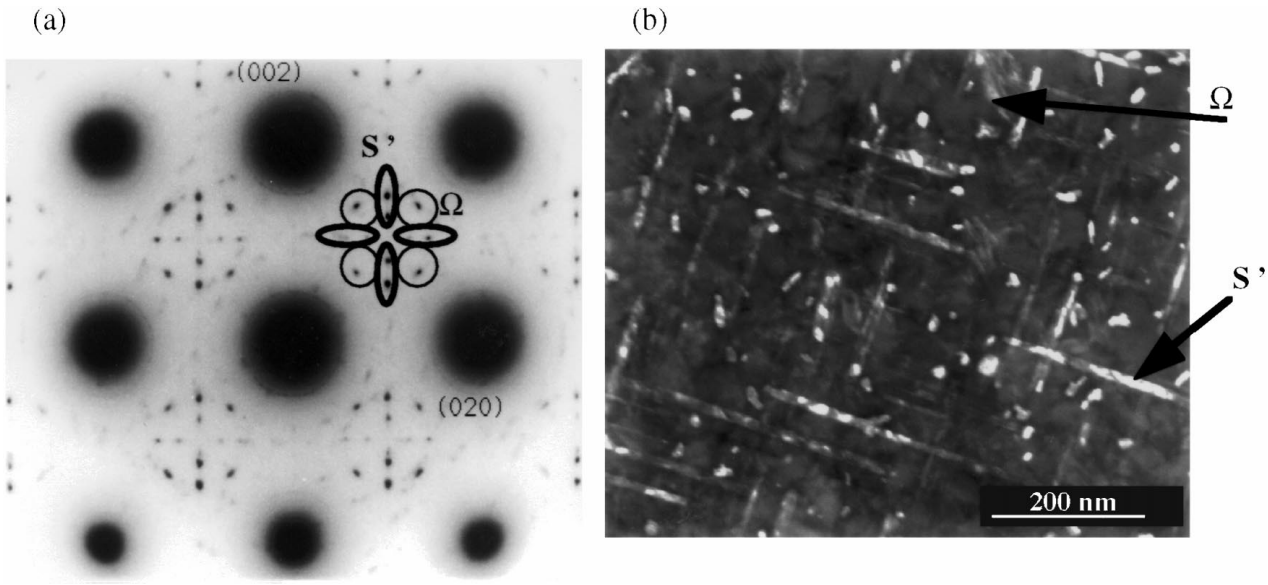

Figure 6 Unreinforced alloy Al4CuMg1Ag (T6): (a) Diffraction pattern in $[100]_\alpha$ direction and (b) dark field image on S′ spot with Ω in the background (also visible, the objective aperture size is too large to select only the S′ spots).

becomes evident by orienting the sample in the $[10\sqrt{2}]_\alpha$ direction, as shown in Fig. 8. Fig. 8a gives the orientation relationship between the lattice structures of α-Al and θ'. Because of the tetragonal structure of θ' ($a = 0.404\,\text{nm}, c = 0.58\,\text{nm} = \sqrt{2}\,a$), the $[10\sqrt{2}]_\alpha$ direction corresponds to $[101]_{\theta'}$ and $[201]_{\theta'}$ directions of θ' plates oriented in $(100)_{\theta'}$ and $(001)_{\theta'}$ planes, respectively, and accordingly designated as θ'_x and θ'_z in Fig. 8a. A program written in Mathematica and linked to EMS [15] was developed to draw diffraction patterns of phases in a matrix. The results of the simulation are in good agreement with the experimental findings as comparatively presented in Fig. 8b and d.

The dark field image with the spot $(111)_\alpha$, which includes the $(11\bar{2})_{\theta' x}$ spot in $[100]_\alpha$ direction, reveals the θ'_x precipitates (Fig. 8c). The rhombus shape of the

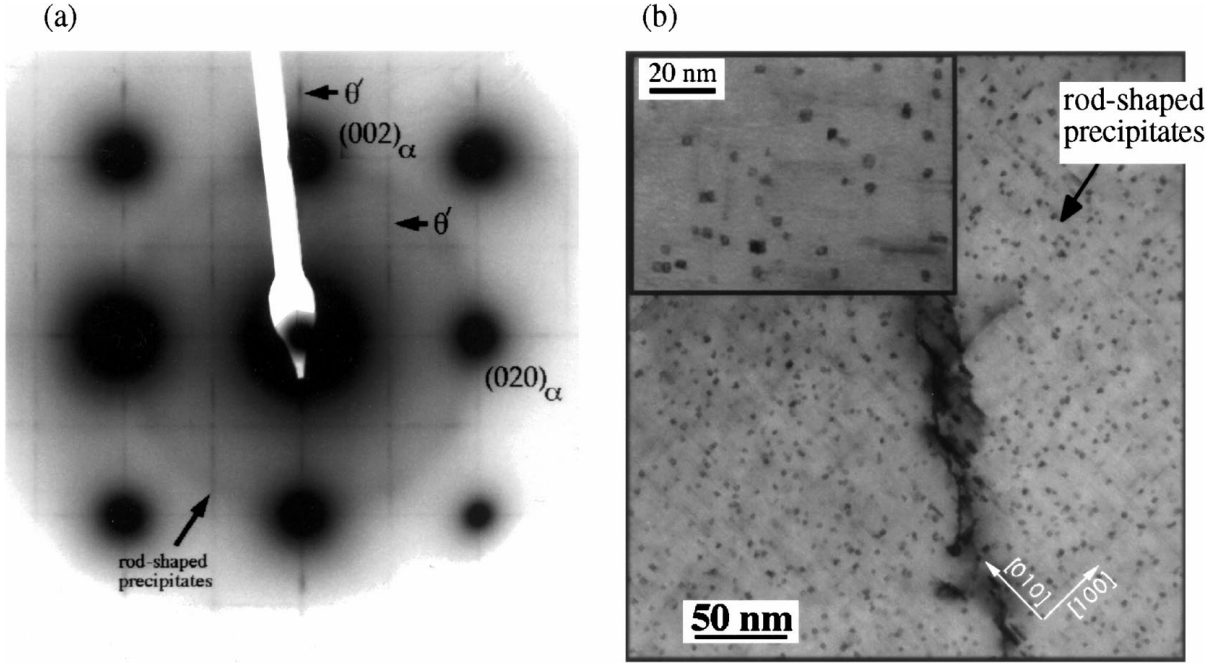

Figure 7 Matrix of the MMC-T6: (a) Diffraction pattern in $[100]_\alpha$ direction and (b) two bright field images of rod-shaped precipitates with θ' in the background close to $[100]_\alpha$.

θ' precipitates on the dark field image corresponds to the square shape of θ' precipitates with sides along {110} and projected on the plane perpendicular to the $[10\sqrt{2}]_\alpha$ direction (electron beam direction) as illustrated for θ'_z in Fig. 8e. The measured acute angles of the rhombus (62°) are in agreement with the predicted α_{shape} (Fig. 8e) as given by the formula:

$$\alpha_{\text{shape}} = 2.\arctan[\cos(\alpha_{\text{tilt}})] = 60^\circ \text{ for } \alpha_{\text{tilt}} = 45^\circ + 9.5^\circ \text{ which corresponds to } \theta'_x \quad (3)$$

Furthermore, contrary to previous reports [3], no precipitation-free zones nor abnormal high densities of θ' precipitates nucleated on dislocation loops in the vicinity of the fibers-matrix interfaces have been observed in the present TEM investigation.

2. The fine and dense rod-shaped precipitates with a square cross-section (1.5×1.5 nm^2) are shown in Fig. 7b. In the dark field image (Fig. 8c), they appear in the background. Some of them seem laying on θ' phase along $\langle 100\rangle_\alpha$ directions. Their length was estimated as 20 nm. After thickness determination of the observation zone with thickness fringes, the density was estimated at 10^{16} cm^{-3}. Their fine size and rod shape make it difficult to determine their crystallographic structure and chemical composition with the classical TEM methods or HREM. Note that the fast Fourier transformations (FFT) of HREM images of some of these precipitates (Fig. 11c) correspond to those of the QP phase described in section 3.5.2 (compare Fig. 11c), suggesting that their structures, are close to one of the QP phase.

3.5. Identification of rod-shaped phase

The composite specimens were overaged at 300 °C for 24 h to artificially coarsen the rod-shaped precipitates. Thus, the characterization of these precipitates becomes possible with HREM, annular dark field observations by scanning transmission electron microscopy (STEM ADF), and EDS. However, since this overageing procedure at 300 °C is prone to affect the nature (crystallography and composition) of the precipitate, the interpretation of the results must be considered with precaution. To avoid misinterpretation and to assess the microstructural evolution, a second overageing treatment was performed at 175 °C for 630 h.

3.5.1. Overageing at 300 °C for 24 h

After this heat treatment, the rod-shaped precipitates were found with two different cross-sections: rectangular and globular (average size 25 nm). As shown in Fig. 9, they are observed as isolated precipitates. Most of them do not lie along θ' precipitates (see for comparison Fig. 10a). EDS analysis and indexing of HREM image (Fig. 9b) reveal, respectively, their chemistry and crystal structure, which are in good agreement with the Q-phase (see section 3.2.1). For the rectangular precipitates, SAED and HREM images prove that their orientation relationship with the aluminium matrix is:

$$[001]_Q // [001]_\alpha, (210)_Q // (100)_\alpha \quad (4)$$

This orientation relationship has been reported in [12], and also given by [16] for the M-phase (crystallographic structure similar to the Q-phase, contains only Al, Mg, Si) but written under an equivalent form allowing to understand the rectangular shape by minimization of the interface misfits:

$$(0001)_Q // (100)_\alpha, [11\bar{2}0]_Q // [510]_\alpha \quad (5)$$

The globular Q phase has also its hexagonal $[001]_Q$ axis parallel to $[001]_\alpha$, but the orientation relationship in its basal plane is more complex.

3.5.2. Overageing at 175 °C for 630 h

Two types of rod-shaped precipitates with a rectangular cross-section (maximum size 8 nm), but different chemical composition, have been distinguished by EDS after overageing at 175 °C for 630 h.

1. One type of these precipitates is always found along the θ' phase as shown in the annular dark field image (Fig. 10a). EDS analysis on these precipitates in thin parts of the sample, which reveals a high Si content (more than 60% wt, Fig. 10b), and the crystallographic features as derived from HREM image Fig. 10d are in agreement with the Si structure. Therefore, it can be concluded that this type of rod-shaped precipitate is Si phase. Si is coherent with the aluminium matrix, with an orientation relationship as follows:

$$[001]_\alpha // [1\bar{1}0]_{Si}, [010]_\alpha // [111]_{Si}, [100]_\alpha // [11\bar{2}]_{Si}, \quad (6)$$

The third orientation relation is deduced from the two first ones, it represents the Al and Si zone axes of Fig. 10c and is coherent with the Si interplanar distances deduced from the translation Moiré fringes corresponding to the $(\bar{2}20)_{Si}$ plans:

$$D_{Moiré} = 3.4\,nm \Rightarrow d_{prec} = \frac{d_\alpha \times D_{Moiré}}{d_\alpha + D_{Moiré}} = 0.191\,nm = d_{220}Si \quad (7)$$

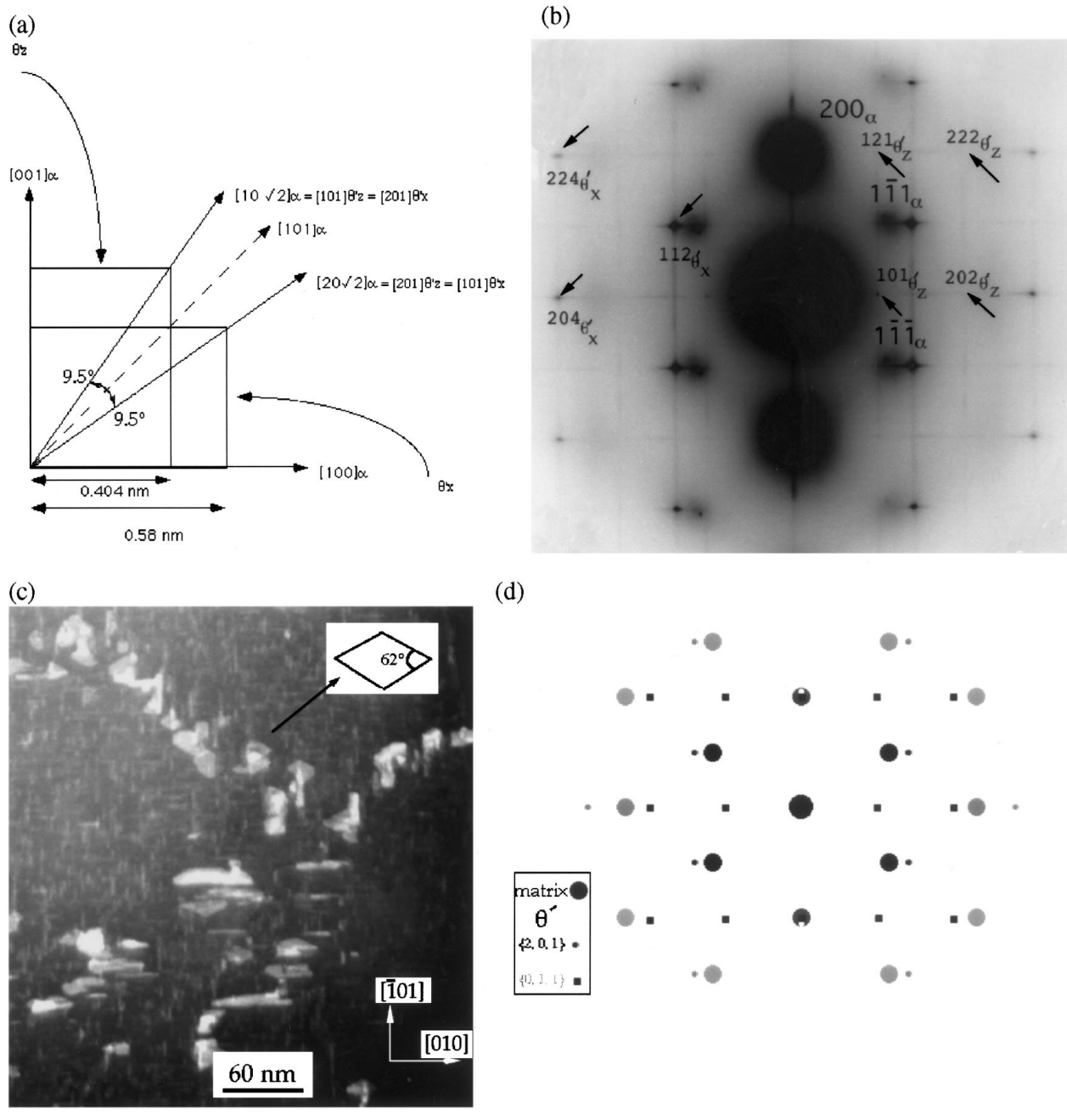

Figure 8 Matrix of the MMC-T6. Diffraction of θ' in $[10\sqrt{2}]_\alpha$ direction: (a) Orientations scheme, (b) diffraction pattern, the $\{111\}_\alpha$ are only visible as blurred spots because of the angle of about 9° between electron beam direction and $[101]_\alpha$ zone axe, (c) dark field image on $(111)_\alpha$ spot, (d) diagram and (e) explanation scheme of the θ' shape in $[10\sqrt{2}]_\alpha$ direction. (*Continued*).

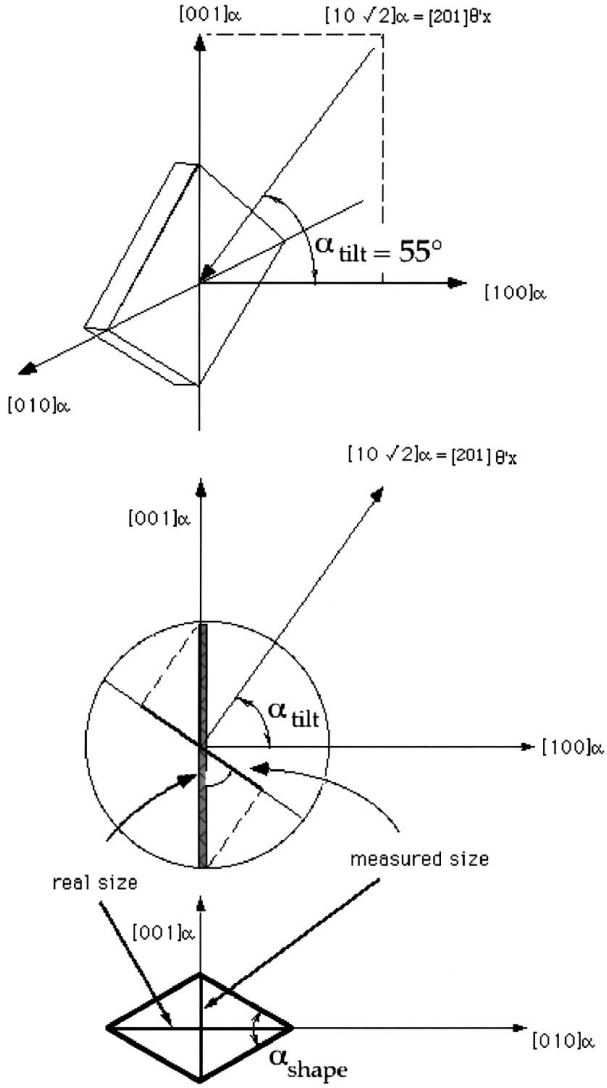

Figure 8 (*Continued*).

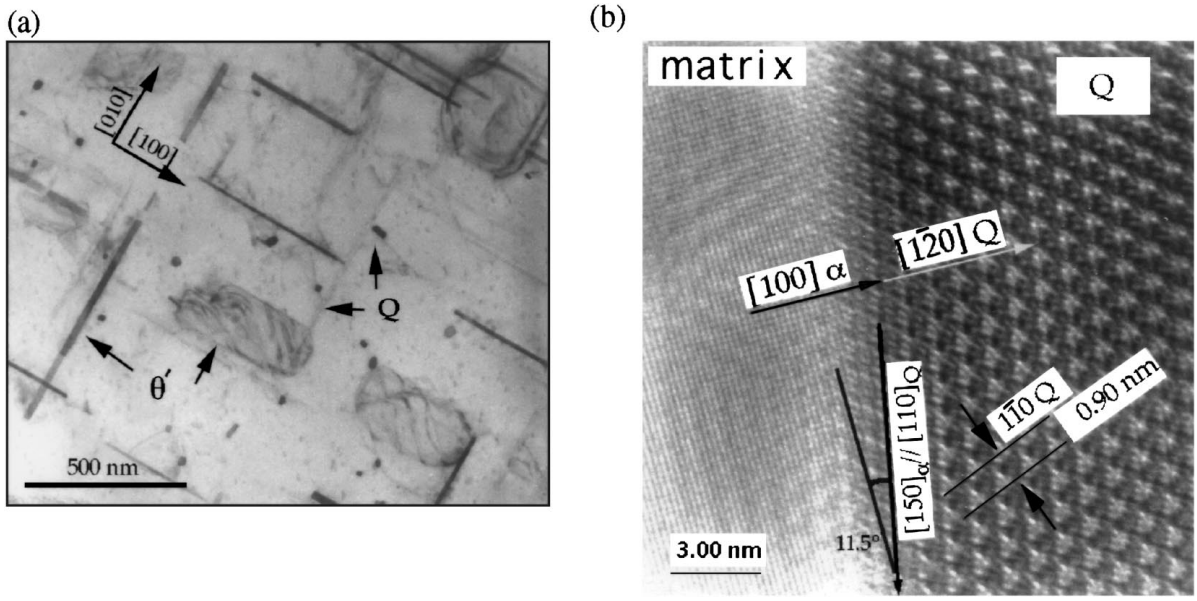

Figure 9 300 °C/24 h overaged MMC: Q phase: (a) Bright field image and (b) HREM image in $[001]_Q$ // $[001]_\alpha$ direction.

The smallest misfit corresponding to the $(001)_\alpha$ // $(1\bar{1}0)_{Si}$ planes (5.2%) is associated with the rod orientation in $[1\bar{1}0]_{Si}$, direction. The orientation relationship (6) is one of those reported by Rosenbaum in his study of the precipitation Si plate-like particles in Al-Si alloys [17].

2. The other type of rod-shaped precipitate contains Al, Mg, Si, and Cu. The Mg/Cu and Si/Cu ratios

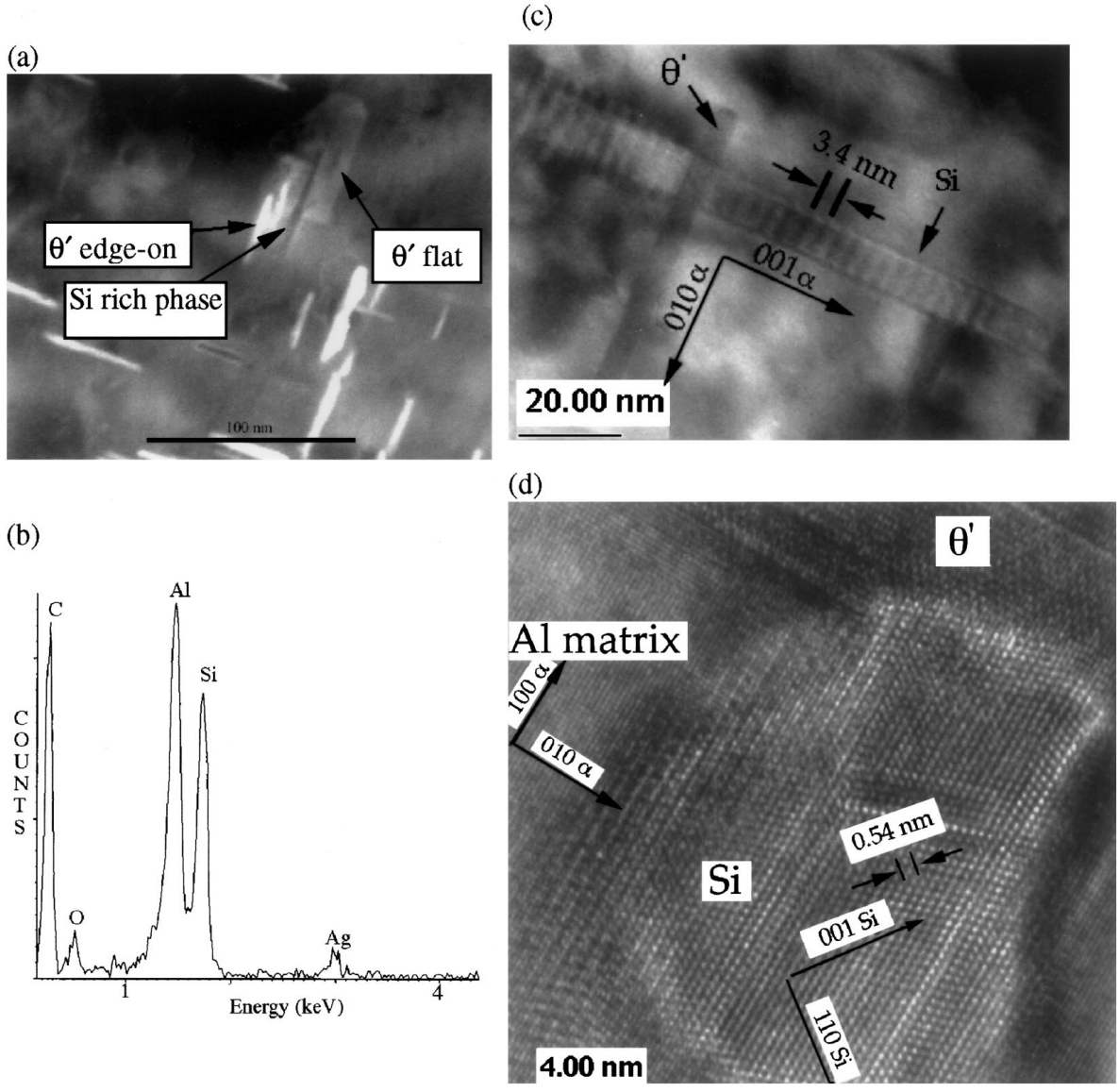

Figure 10 175 °C/630 h overaged MMC: Si rod-shaped precipitates: (a) STEM ADF image in $[001]_\alpha$ direction, (b) correspondent EDS spectrum, and (c) bright field image with Moiré fringes, and (d) HREM image in $[001]_\alpha$ // $[1\bar{1}0]_{Si}$ direction.

measured on four precipitates of this type range between 3.5–4.5 and 2–4, respectively, and are close to those of Q-phase (4 and 3). Nevertheless, HREM images are not in agreement the Q lattice parameters as shown in Fig. 11a. Instead, an hexagonal arrangement with $a = 0.395\ \text{nm} \pm 0.01\ \text{nm}$ is visible on the HREM filtered image (the FFT of the image and the filter are shown Fig. 11b). This phase is noted QP. Its following orientation relationship with α-Al is:

$$[100]_{QP}//[010]_\alpha \text{ and } [001]_{QP}//[001]_\alpha \qquad (8)$$

This phase is noted QP because these precipitates are not situated on θ' plates (unlike the Si rod-shaped precipitates) as are the Q precipitates found by overageing 300 °C for 24 h, and because their chemical composition is close to that of Q phase, suggesting that this phase is a Q-phase precursor. Further investigation has been planned to verify this assumption.

4. Discussion

4.1. SiO_2 reduction and Si diffusion

The initial composite matrix alloy is virtually free of Si (0.043%). Considering the expected reactivity of the SiO_2 binder in the preform with Mg contained in the alloy melt, the presence of Si in the matrix is obviously the result of a binder-matrix chemical reaction that releases Si from the binder into the matrix [6, 18, 19, 20, 21, 22]. The possible reactions associated with the Si release and the Mg depletion in the matrix are reported as follows:

$$Mg + 1/2\,SiO_2 \rightarrow MgO + 1/2\,Si \qquad (9)$$

$$Mg + 2SiO_2 + Al \rightarrow MgAl_2O_4 + 2Si \qquad (10)$$

The two products of reaction (MgO and $MgAl_2O_4$) are effectively present in the MMC-T6 sample: MgO in the core part and $MgAl_2O_4$ in the surface of the reacted binder. The presence of large $MgAl_2O_4$ spinels substituting the SiO_2 binder in the MMC-F sample proves that the reduction of the binder occurs during the infiltration of the preform. The silicon released from the reaction forms coarse insoluble precipitates as Q phase, or diffuses into the matrix during the heat treatment to form the rod-shaped precipitates, as described earlier.

According to the SiO_2 binder content, the complete reaction of the SiO_2 in the binder can only provide

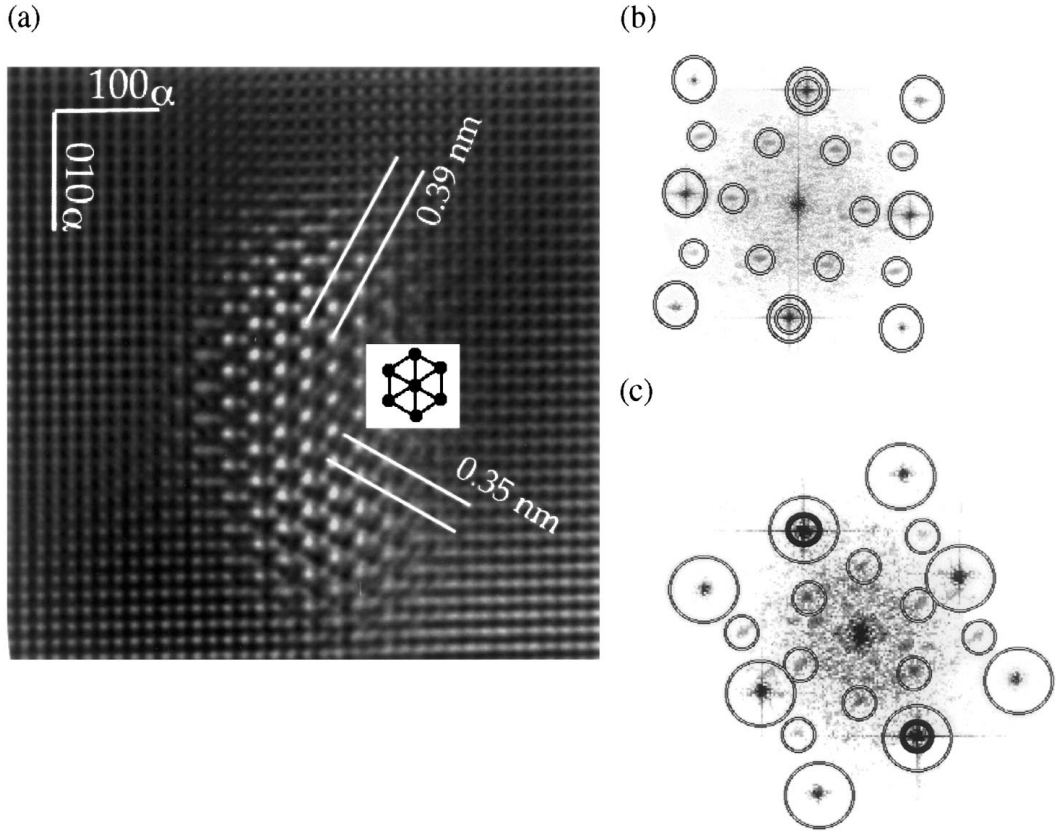

Figure 11 175 °C/630 h overaged MMC: QP rod-shaped precipitates: (a) Filtered HREM image on $[100]_\alpha$ direction and (b) FFT of the HREM image with the corresponding filter. For comparison: (c) FFT of HREM image obtained on the rod-shaped precipitates in the MMC-T6 specimen.

0.3% wt of Si to the matrix (the binder represents 5 wt % of the fibers and the fibers 15% vol of the material). This is considerably lower than the 0.6–0.9% wt found in the matrix by EDS analyses. Considering the fact of SiO_2 bearing of the Saffil fibers (3–4 wt % of fibers), a small amount of this SiO_2 in the fibers may also react with Mg and provide about 0.3% wt of Si to the matrix. This is confirmed by EDS analysis on a second composite of AlCu4Mg1Ag alloy, reinforced with a Saffil preform containing Al_2O_3 binder, and fabricated with the same processing conditions. The analysis results reveal a Si content of 1% wt in the fibers and 0.2% wt in the matrix. Thus, it can be concluded that Si comes not only from the SiO_2 binder but also from the SiO_2 containing δ-Al_2O_3 fibers; these two Si sources lead to the high content of Si measured in the matrix.

4.2. Fine precipitation

The presence of Si and the depletion of Mg in the matrix changes the location of the matrix chemical composition in the Al-Cu-Mg-Si phase diagram. Ω and S′, the two main phases in the monolithic AlCu4Mg1Ag-alloy, do not appear in the composite matrix. Instead, θ' phase, which is not detected in the unreinforced alloy, becomes the main precipitation phase together with rod-shaped precipitates. Moreover, during prolonged overageing (175 °C/630 h) Si rod-shaped precipitates and a high density of rod-shaped precipitates containing Al, Cu, Mg, Si, probably a precursor of Q-phase, are found in the matrix. These observations are in agreement with the equilibrium Al-Cu-Mg-Si phase diagram [9], which reports the coexistence of the Q, Si, and θ phases for the composition: 4% wt Cu, 0.6% wt Si, 0.5% wt Mg.

The change of the precipitation state is obviously due to the apparition of Si, more than the depletion of Mg. In fact, the precipitation change identified in the present study is similar to that observed by Gupta [23] and Gao [24]. Gao studied the effects of Si additions in Al-Cu-Mg alloys, and reported a complete suppression of Ω and S′ phases, and a coexistence of fine-scale distribution of θ' and Q phases (Q was determined by overageing). The microstructure change was associated with an improvement of the mechanical properties [25, 26].

The microstructure change between the unreinforced alloy and the composite resulting from the reduction of the SiO_2 binder and the resultant Si migration into the matrix was reported by Schueller [22] for AlCu4Mg2 reinforced by Al_2O_3-Saffil fibers or SiC whiskers. He observed the apparition of a new phase σ-$Al_5Cu_6Mg_2$, in addition to the dense θ' precipitation. The explanation proposed by Schueller is based on the possible existence of Si clusters, which create compressive strain in the matrix and attract a high concentration of small Cu atoms to their interfaces. This hypothesis is confirmed in the present study, although the Si rod-shaped precipitates are not in their initial "cluster" state, possibly a consequence of the heat treatment.

The complementary role of Si and Cu on the precipitation state is confirmed by the studies on the effect of Cu addition on the precipitation in Al-Mg-Si alloys [27, 28]. These studies reported an improvement in mechanical properties due to a denser precipitation state. Moreover, the precipitation state of Al-Cu-Mg with Si addition and Al-Mg-Si with Cu addition feature similar diffraction patterns and bright field images. Even if the

predominant phases are θ' in the 2xxx alloys and β'' (precursor of the Mg_2Si phase) in the 6xxx alloys, the precipitation in the two types of alloys is characterized by the apparition of thin rod-shaped precipitates. Due to their role in the enhancement of the mechanical properties, these rod-shaped precipitates have been intensively studied in the 6xxx alloys [28–31]. The fineness of the precipitation (few nanometers) makes their crystallographic and chemical identification difficult. However, it is possible to extract them from the alloy by a preferential matrix dissolution technique, which permits their characterization by conventional TEM techniques as reported by Matsuda [32]. The rod-shaped precipitates containing Al, Cu, Mg, and Si observed in the present study are not mentioned in the literature; with respect to shape and elemental constitution, the closest precipitate having been reported is L phase in 6xxx alloys containing Cu [30]. Further HREM studies of these precipitates by extraction replica are in preparation.

5. Conclusion

In the present study, the effect of preform-matrix chemical reaction on the precipitation state of the matrix in a SiO_2 binder containing Saffil preform reinforced AlCu4Mg1Ag alloy is examined. We find that the interfacial reaction between Mg in the matrix alloy and SiO_2 in the preform results in double atom migration: Mg migrates into fiber binder, and Si is released into the matrix. The reaction product at the interfaces are the magnesium oxide MgO and the spinel $MgAl_2O_4$. The precipitation state of the monolithic matrix alloy

$$\alpha.\mathrm{liq} \rightarrow \Omega + \mathrm{S}' + \theta' \rightarrow \Omega + \mathrm{S} + \theta \qquad (13)$$

is modified by the presence of Si. The precipitation sequence observed in the AlCu4Mg1Ag/Saffil composite matrix is:

$$\alpha.\mathrm{liq} + \mathrm{Si} \rightarrow \theta' + \text{rod-shaped precipitates (peak aged)} \qquad (14)$$

$$\alpha.\mathrm{liq} + \mathrm{Si} \rightarrow \mathrm{QP} + \mathrm{Si} + \theta' \qquad (175\,^{\circ}\mathrm{C}/630\,\mathrm{h}) \qquad (15)$$

$$\alpha.\mathrm{liq} + \mathrm{Si} \rightarrow \mathrm{Q} + \theta' + \theta \qquad (300\,^{\circ}\mathrm{C}/24\,\mathrm{h}) \qquad (16)$$

In the MMC matrix overaged at 175 °C during 630 h, Si appears as rod-shaped precipitates (5 nm × 10 nm × 50 nm) on θ' plates, which confirms the hypothesis of Si clusters favoring fine precipitation of θ' during the early stages of ageing. Its orientation relationships with the Al matrix are $[001]_\alpha // [1\mathbf{1}0]_{Si}$, $[010]_\alpha // [111]_{Si}$, $[100]\alpha // [112]_{Si}$, and the rod direction is $[001]_\alpha // [1\mathbf{1}0]_{Si}$ and is associated with the smallest misfit (5.2%). Another type of rod-shaped precipitate, possibly precursor of the Q phase, containing Al, Cu, Mg, and Si, presenting an hexagonal arrangement with $a = 0.395$ nm, and noted QP, is also observed. The rod-shaped precipitates present in the peak-aged MMC seem to have a structure close to the one of the QP phase; further investigations have to be done to identify them more precisely.

Acknowledgements

The authors acknowledge Prof. P. Stadelmann and Dr. L. Sagalowicz for their encouraging and interesting discussions, A. Merglen and S. Bonjour for their help in preparing TEM samples, and A. Sfera and M. Foeth for their support.

References

1. J. ELIASSON and R. SANDSTRÖM, *Key Eng. Mater.* **104-107** (1995) 3.
2. D. SCOTT, R. L. TRUMPER and MING YANG, *Comp. Sci. Technol.* **42** (1991) 251.
3. T. W. CLYNE and P. J. WITHERS, in "An Introduction to Metal Matrix Composites," (Cambridge University Press, Cambridge, 1993), pp. 370–398.
4. J. BÄR, H. J. GUDLADT *et al., Mater. Sci. Forum* **217-222** (1996) 1145.
5. P. VERMAUT and P. RUTERANA, *J. Microsc.* **177** (1995) 387.
6. J. M. ROURKE, R. S. BUSHY and V. D. SCOTT, *Comp. Sci. Technol.* **56** (1996) 957.
7. *Idem, ibid.* 1071.
8. O. BEFFORT, C. SOLENTHALER *et al., Mater. Sci. Engng.* **A191** (1995) 121.
9. L. F. MONDOLFO, in "Aluminium alloys, structure and properties" (Butterworth, 1st edition, London, 1976).
10. L. ARNBERG and B. AURIVILLIUS, *Acta. Chem. Scand.* **A34** (1980) 1.
11. A. K. GUPTA, A. K. JENA and M. C. CHATURVEDI, *Mater. Sci. Tech.* **3** (1987) 1012.
12. B. DUBOST, J. BOUVAIST and M. REBOUL, in Proceedings of the 1st International Conference on Aluminium Alloys, edited by E. A. Starke and T. H. Sanders (1986) p. 1109.
13. JCPDS-ICDD Software, International Center for Diffraction Data, Pennsylvania (1987).
14. W. B. PEARSON in "A Handbook of lattice spacings and structures of metals and alloys" (Pergamon Press, Belfast, 1958).
15. P. STADELMANN, *Ultramicroscopy* **21** (1987) 131.
16. L. SAGALOWICZ, G. LAPASSET and G. HUG, *Phil. Mag. Letters* **74** (1996) 57.
17. H. S. ROSENBAUM and D. TURNBULL, *Acta Metall.* **7** (1959) 664.
18. R. MOLLINS, J. D. BARTOUT and Y. BIENVENU, *Mater. Sci. Engng.* **A135** (1991) 111.
19. H. J. DUDEK *et al., ibid.* **A167** (1993) 129.
20. SHUNCAI WANG *et al.*, Z. *Metallkd.* **86** (1995) 2.
21. J. C. LEE *et al.*, Metall. Trans. A **28A** (1997) 1251.
22. R. D SCHUELLER, F. E WAWNER and A. K. SACHDEV, *J. Mater. Sci.* **29** (1994) 424.
23. A. K. GUPTA, M. C. CHATURVEDI and A. K. JENA, *Mater. Sci. Tech.* **5** (1989) 52.
24. X.GAO, J. F. NIE and B. C. MUDDLE, *Mater. Sci. Forum.* **217-222** (1996) 1251.
25. R. N. WILSON, D. M. MOORE and P. J. E. FORSYTH, *J. Inst. Metals* **95** (1967) 177.
26. M. TAMIZIFAR and G. W. LORIMER, in Proceedings of the 3rd International Conference on Aluminium Alloys, (1992) p. 220.
27. TAKEO SAKURAI and TAKEHIKO ETO, in Proceedings of the 3rd International Conference on Aluminium Alloys, (1992) p. 208.
28. S. P. RINGER *et al., Mater. Sci. Forum* **217-222** (1996) 689.
29. JI-YONG YAO, G. A. EDWARDS and D. A. GRAHAM, *ibid.* **217-222** (1996) 777.
30. L. SAGALOWICZ *et al.*, in Proceedings of the 4th International Conference on Aluminium Alloys, (1994) p. 636.
31. KENJI MATSUDA *et al., Mater. Sci. Forum* **217-222** (1996) 707.
32. *Idem. Scripta Metall. et Mater.* **32** (1995) 1175.

Received 1 June
and accepted 26 August 1998